

A study of gamma-ray burst afterglows as they first come into view of the Swift Ultraviolet and Optical Telescope

M.J. Page¹, S.R. Oates^{2,1}, M. De Pasquale^{3,1}, A.A. Breeveld¹, S.W.K. Emery¹, N.P.M. Kuin¹, F.E. Marshall⁴, M.H. Siegel⁵, P.W.A. Roming⁶

¹*Mullard Space Science Laboratory, University College London, Holmbury St Mary, Dorking, Surrey, RH5 6NT, UK*

²*Department of Physics, University of Warwick, Coventry CV4 7AL, UK*

³*Department of Astronomy and Space Sciences, Istanbul University, Turkey*

⁴*Astrophysics Science Division, NASA Goddard Space Flight Centre, Greenbelt MD, 20771 USA*

⁵*Department of Astronomy and Astrophysics, The Pennsylvania State University, University Park, PA 16802, USA*

⁶*Southwest Research Institute Space Science and Engineering Division, 6220 Culebra Road San Antonio, TX 78238-5166, USA*

Accepted —. Received —; in original form —

ABSTRACT

We examine the the emission from optically bright gamma-ray burst (GRB) afterglows as the Ultraviolet and Optical Telescope (UVOT) on the *Neil Gehrels Swift Observatory* first begins observing, following the slew to target the GRB, while the pointing of the *Swift* satellite is still settling. We verify the photometric quality of the UVOT settling data using bright stars in the field of view. In the majority of cases we find no problems with the settling exposure photometry, but in one case we excise the first second of the exposure to mitigate a spacecraft attitude reconstruction issue, and in a second case we exclude the first second of the exposure in which the UVOT photocathode voltage appears to be ramping up. Of a sample of 23 afterglows which have peak V magnitudes < 16 , we find that all are detected in the settling exposures, when *Swift* arrives on target. For 9 of the GRBs the UVOT settling exposure took place before the conclusion of the prompt gamma-ray emission. Five of these GRBs have well defined optical peaks after the settling exposures, with rises of > 0.5 mag in their optical lightcurves, and there is a marginal trend for these GRBs to have long T_{90} . Such a trend is expected for thick-shell afterglows, but the temporal indices of the optical rises and the timing of the optical peaks appear to rule out thick shells.

Key words: gamma-ray bursts : general

1 INTRODUCTION

Gamma-ray bursts are the most powerful cosmic explosions. They are observed as transient sources of gamma-rays, which typically last between 10^{-2} and 10^3 s (Kouveliotou, 1994). This gamma-ray emission, which is usually referred to as the *prompt* gamma-ray emission, is followed by a longer lasting afterglow from X-ray to radio wavelengths (e.g. De Pasquale et al., 2006). The standard paradigm for the prompt emission is that it arises from shocks associated with the collisions of shells ejected with different Lorentz factors in a highly relativistic explosion. The radiation generation mechanism(s) for the prompt emission remain the subject of debate, with possibilities including synchrotron emission from the shocks (e.g. Rees & Mészáros, 1994), Compton upscattering of photospheric emission (e.g. Rees & Mészáros, 2005) or magnetic reconnection (e.g. Zhang & Yan, 2011). The

emission in these models is often described as internal emission because it takes place within the relativistic ejecta, before the ejecta are slowed significantly through interaction with the surrounding medium. The afterglow is thought to originate in the shocks arising from the collision of the ejecta with the surrounding interstellar medium; these shocks are therefore described as the external shocks (Rees & Mészáros, 1992).

Observational data are most constraining for models of the prompt emission and afterglow when the afterglow observations are obtained very quickly after, if not simultaneously with, the prompt emission. The *Neil Gehrels Swift Observatory* (hereafter *Swift*) carries a suite of instruments on a platform with rapid repointing capabilities and a significant degree of autonomy to permit the study of GRBs and their early afterglow emission (Gehrels et al., 2004). *Swift* begins its afterglow observations most rapidly when it

detects and localises GRBs on-board with the Burst Alert Telescope (BAT; Barthelmy et al., 2005), prompting *Swift* to execute an automatic slew to point the Ultraviolet and Optical Telescope (UVOT; Roming et al., 2005) and X-ray Telescope (XRT; Burrows et al., 2005) at the target. Response times of 1-2 minutes are common.

During the slew, the UVOT is protected from damage by bright stars passing through the field of view by maintaining the photocathode in a low-voltage state. At the conclusion of the slew, *Swift* signals to the UVOT that it has arrived at the target, and the UVOT begins its first exposure. At this point, *Swift's* reaction wheels are stabilising the satellite, such that the pointing direction is in transition from a motion of many arcseconds per second to a stable pointing. The exposure taken by UVOT during this transition is known as the settling exposure; its nominal duration is 10 s. The settling exposure is almost always taken through the *V* filter; exceptions are found in a small period at the beginning of the mission when the default settling filter was UVM2, and occasions when the field of view of UVOT contains one or more stars which are recorded in the on-board catalogue as being too bright for safe observations through the *V* filter.

Despite being the earliest UVOT exposure of *Swift*-discovered GRBs, the settling exposure is frequently ignored or discarded (e.g. Oates et al., 2012). The main reason is that photometry derived from the settling exposure is regarded as uncertain because of the changing UVOT photocathode voltage at the beginning of the exposure; the rapidly changing spacecraft attitude can also be a cause for concern (Roming et al., 2017). The settling exposure usually begins 10-15 seconds before the first settled exposure, and so represents a significant shifting forward of the afterglow observations, if the photometry can be trusted.

The detector of the UVOT is a micro-channel plate (MCP) intensified charge coupled device (CCD) (MIC; Fordham et al., 1989). It detects the photons individually with a time resolution limited by the frame time of the CCD, which is usually 11 ms. Data can be recorded and relayed to the ground as event lists, in which the arrival times and positions of the individual photons are retained, or as an image accumulated over a time interval. To meet data and telemetry limits, most UVOT data are recorded as images. Settling exposures are recorded as event lists. Although the satellite is moving during the settling exposure, the changing attitude of the satellite is taken into account when the photons are assigned sky coordinates. Thus an image of the sky can be constructed from the settling-exposure event list in which stars have shapes consistent with the normal UVOT point spread function, and there is no evidence of trailing.

In this paper, we verify the photometric quality of the settling exposures of a group of relatively bright GRB afterglows observed with *Swift* UVOT. Photometry of the GRB afterglows is then derived from the settling exposures, and the implications of these very early data are examined. In Section 2 we describe the sample selection, observations and data reduction. Our results are presented in Section 3 and discussed in Section 4. Our conclusions are given in Section 5. An appendix provides the measurements which were used to verify the photometric quality of the settling exposures. All magnitudes are given in the UVOT Vega system (Poole et al., 2008). All GRB times are referenced to the

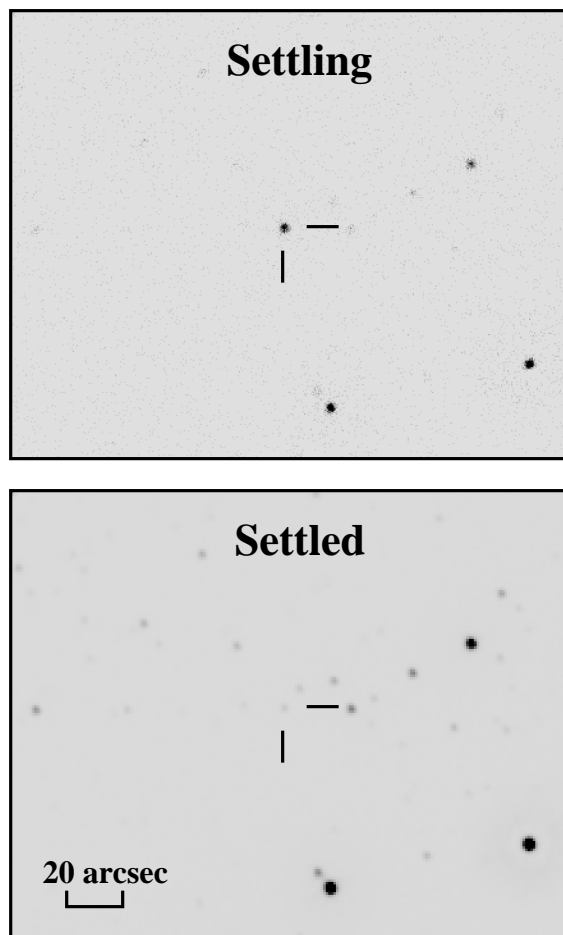


Figure 1. Examples of settling (top) and settled (bottom) images for GRB 050525A, constructed via the procedure described in Section 2.2. Note that only a fraction of the UVOT field of view is shown. The GRB afterglow is marked at the centre. The pixel size for the settling image is $0.5 \text{ arcsec} \times 0.5 \text{ arcsec}$, because the UVOT event list retains the full spatial sampling of the UVOT detector array, while the settled image has $1 \text{ arcsec} \times 1 \text{ arcsec}$ pixels, reflecting the on-board 2×2 binning usually employed for image-mode data.

beginning of T_{90} , which is the time period containing 90 per cent of the gamma-ray emission, as recorded in the *Swift* BAT on-line processing¹.

2 SAMPLE SELECTION, OBSERVATIONS AND DATA REDUCTION

2.1 Sample Selection

Our objective is to examine the early periods of gamma-ray burst optical afterglow light curves to determine what fraction of the sample shows significant afterglow emission when *Swift* UVOT first arrives on target. Therefore we require a sample of gamma-ray burst afterglows that (a) are optically bright enough that we can expect to detect the afterglow in settling observations at a significant fraction of

¹ http://gcn.gsfc.nasa.gov/swift_gnd_ana.html

the peak flux, (b) were observed soon after the trigger and (c) have redshifts so that their observed properties can be transformed to the rest-frame.

With these criteria in mind, we have started with the sample of GRBs studied by Oates et al. (2012). The sample of Oates et al. (2012) was drawn from the second UVOT GRB catalogue (Roming et al., 2017), which contains all of the GRBs observed with *Swift* UVOT from the launch of *Swift* until 25 December 2010. For inclusion in their sample, Oates et al. (2012) required that a GRB must have been observed by UVOT within the first 400s after the BAT trigger and have a measurement of redshift, reflecting our criteria (b) and (c). For a typical settling exposure duration of 10 s, the limiting magnitude for a measurement with a signal to noise of 3 is $V = 17.5$ mag. Our criterion (a) must therefore be more stringent than the peak brightness limit ($V \leq 17.89$ mag) adopted by Oates et al. (2012). For our study we have included only objects which have a peak V magnitude of ≤ 16.0 , which corresponds to a sample of 23 GRBs that are listed in Table 1.

2.2 Observations, data reduction and analysis

All of the GRBs in the sample were observed with *Swift* UVOT in Automated Target (AT) mode, and the analysis is restricted to those observations obtained in the initial observing segment, roughly the first 24 hours from the detection of the burst.

For each GRB the UVOT V -band sky images and event data were retrieved from the UK *Swift* Science Data Centre². Images were screened visually for problems such as source trailing and any affected images were discarded. Then, for each GRB all remaining images except for that of the settling exposure were summed using the standard *Swift* FTOOL task UVOTISUM to produce a single settled image. For the settling exposures, sky images were constructed from the event lists using EVSELECT. The resulting sky images were inspected for attitude problems indicated by trailing of stars. Only in the case of GRB 061007 was a problem identified; in this case the problem was solved by discarding the first second of the settling exposure. Then, for each GRB the settling image and settled image were registered and aspect corrected to the same astrometric reference frame using the USNO-A2.0 source catalogue (Monet et al., 1998). Examples of the settling and settled images constructed in this way are shown in Fig. 1.

Photometric measurements of between one and 3 reference stars in the settling and settled images of each GRB field were then obtained to assess the photometric properties of the settling images. The brightest non-saturated stars in each field were chosen as the reference stars in order to maximise the accuracy of the photometry. Circular apertures of 5 arcsec radius were employed for the source measurements, as is standard practice for measurement of bright sources in UVOT (Poole et al., 2008), and background was measured from a source-free circular aperture of 25 arcsec radius. The measurements were carried out with the standard *Swift* FTOOL task UVOTMAGHIST, which corrects for coincidence-loss, the evolution of the UVOT sensitivity with time, and

the large scale sensitivity variations over the detector (see Breeveld et al., 2010).

Photometric measurements of the GRB afterglows in the settling exposures were carried out by following the same procedure as for the reference stars.

3 RESULTS

Fig. 2 shows the photometric offsets of the settling exposures with respect to the later, settled exposures as measured with the reference stars in each field. Further details of the reference-star measurements are given in Appendix A. The majority of the offsets are negative, indicating that the reference stars appear to be fainter in the settling exposures, but most offsets are small (all but two are below 0.1 magnitude) and only one, corresponding to GRB 091020, is individually significant at $> 2\sigma$. Where a bright enough comparison star is available, we have further investigated the photometric stability of the settling exposures by splitting them into 1 s chunks and generating lightcurves for the comparison stars; the lightcurves are given in Appendix A. In only one case do we see evidence that the ramp-up of the photocathode voltage impinges on the settling exposure: the comparison star in the field of GRB 091020 appears a magnitude fainter in the first second than in the remainder of the settling exposure. This problem can be remedied by excluding the first second of the settling exposure from our analysis. So doing, the photometric offset of the GRB 091020 field changes from -0.13 ± 0.05 to -0.05 ± 0.05 , consistent with zero at 1σ . After this correction to the GRB 091020 field, the weighted mean offset for all GRB fields is -0.021 ± 0.009 mag. This mean offset is sufficiently marginal (2σ) that we cannot distinguish whether it is a genuine instrumental effect or a statistical fluctuation. The size of the mean offset is sufficiently small (less than half of the 1σ uncertainty on the best settling-exposure photometry in our GRB sample) that we do not consider any correction to the settling-exposure photometry to be necessary.

Photometry for the GRBs from the settling exposures are given in Table 1, together with their redshifts, some optical measurements at later times from the lightcurves constructed by Oates et al. (2012), and the T_{90} durations of their gamma-ray emission from the on-line BAT processing¹. All of the GRBs were detected in the settling exposure with a significance of $> 3\sigma$ with respect to the Poisson fluctuations in the background. Note that in the case of GRB 061007, the count rate of the afterglow exceeds the calibrated limit for coincidence-loss correction in UVOT (see Poole et al., 2008; Page et al., 2013) during the settling exposure. Consequently, we report an upper limit for the magnitude, corresponding to the maximum calibrated count rate, in Table 1. In statistical terms, GRB 061007 is securely (3σ) brighter than this limit, using the statistical uncertainties derived by Kuin & Rosen (2008).

Fig. 3 shows the difference between the magnitude recorded in the settling exposure (V_{settle}) and the brightest magnitude recorded either in the settling exposure or the subsequent UVOT lightcurve ($V_{\text{brightest}}$) against the time of the peak optical emission (T_{peak}) in the rest frame of the GRB. When the brightest magnitude for a GRB is recorded in the settling exposure, T_{peak} is shown as an upper limit.

² <http://www.swift.ac.uk>

Table 1. The GRB sample. T_{settle} is mid-time of the settling exposure referenced to the beginning of T_{90} . Redshifts and brightest V magnitudes are those used by Oates et al. (2012), except for GRB080319B, for which the UVOT data were saturated at early times. The brightest V magnitude listed for GRB080319B is the brightest V magnitude from subsequent UVOT observations, obtained by read-out-streak photometry (Page et al., 2013). The settling V magnitude for GRB080319B listed here is the magnitude recorded by TORTORA at the time of the UVOT settling exposure (Racusin et al., 2008).

GRB	Redshift	Brightest V mag post-settling (mag)	Settling V mag (mag)	T_{settle} (s)	T_{90} (s)
GRB 050525A	0.606	13.47 ± 0.06	13.42 ± 0.06	70.2	8.8
GRB 050801	1.38	15.18 ± 0.12	15.49 ± 0.14	56.3	19.4
GRB 050922C	2.198	14.46 ± 0.06	13.92 ± 0.06	104.3	4.5
GRB 060418	1.489	14.58 ± 0.04	15.96 ± 0.17	136.7	144.0
GRB 060607	3.43	14.49 ± 0.04	16.62 ± 0.26	103.5	60.5
GRB 060908	2.43	14.97 ± 0.05	14.70 ± 0.09	75.0	19.3
GRB 061007	1.261	11.93 ± 0.03	< 11.67	72.0	75.3
GRB 061021	0.77	15.46 ± 0.05	15.00 ± 0.11	63.9	46.2
GRB 061121	1.314	15.41 ± 0.05	17.52 ± 0.43	39.5	81.2
GRB 070318	0.836	15.34 ± 0.05	16.18 ± 0.20	58.8	108.0
GRB 080319B	0.937	10.07 ± 0.24	6.43 ± 0.06	51.0	45.1
GRB 080721	2.602	13.41 ± 0.04	12.99 ± 0.06	118.5	64.0
GRB 080810	3.35	13.58 ± 0.04	13.49 ± 0.06	77.1	108.8
GRB 081008	1.967	14.29 ± 0.03	14.37 ± 0.08	125.6	185.5
GRB 081203A	2.05	13.04 ± 0.02	15.87 ± 0.17	93.4	221.0
GRB 081222	2.77	14.93 ± 0.05	12.80 ± 0.06	46.5	33.0
GRB 090401B	3.1	15.22 ± 0.06	14.90 ± 0.11	67.8	186.5
GRB 090424	0.544	14.49 ± 0.04	13.74 ± 0.07	79.7	49.5
GRB 090618	0.54	14.30 ± 0.04	13.97 ± 0.07	105.9	113.2
GRB 090812	2.452	15.66 ± 0.06	15.70 ± 0.15	73.7	66.7
GRB 091018	0.971	14.38 ± 0.06	13.77 ± 0.07	56.0	4.4
GRB 091020	1.71	15.08 ± 0.04	14.86 ± 0.11	80.2	39.0
GRB 100906A	1.727	14.50 ± 0.04	14.11 ± 0.08	73.7	14.3

The majority of the data points are clustered at the bottom left of the figure. For these sources the settling exposure is either the brightest measurement or differs by less than 0.4 mag from the brightest measurement. Away from the bottom left corner are five GRBs which brighten significantly (by 0.5 – 3 mag) after the settling exposure, and therefore have optical lightcurves which show a well defined peak.

Fig. 4 shows the mid-time of the settling exposure T_{settle} against the gamma-ray duration T_{90} , with both times transformed to the rest-frame of the GRB. The solid line indicates $T_{\text{settle}} = T_{90}$. Nine out of 23 points lie below the line, implying that UVOT took its first exposures while the prompt gamma-ray emission was still underway.

4 DISCUSSION

For our sample of 23 GRBs with bright optical afterglows, the optical emission had already begun by the time of the *Swift* UVOT settling exposure in every single case. In 9 cases, the settling exposure took place before the end of the T_{90} period in which most of the prompt gamma rays are emitted. We do not observe a delay between the end of the gamma-ray emission and the beginning of that in the optical in any GRB. Such a statement could be made on the basis of some previous studies of GRB samples with rapid optical follow up (e.g. Rykoff et al., 2009; Oates et al., 2009), but the homogeneity and size of our sample place this conclusion on a firmer statistical footing.

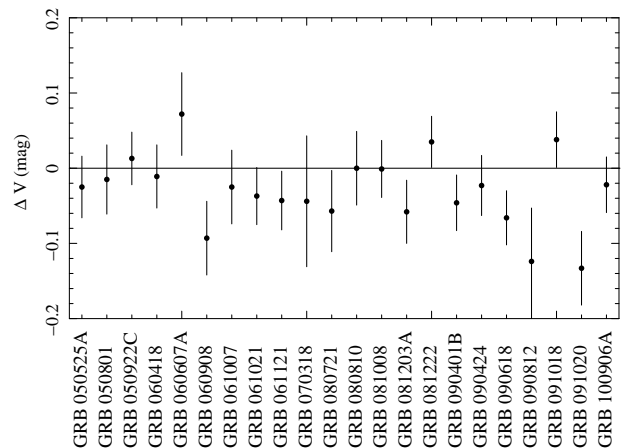


Figure 2. Weighted mean difference ΔV between the magnitudes of the reference stars in the settling and settled exposures for each field. ΔV is computed as $V_{\text{settled}} - V_{\text{settling}}$ where V_{settling} is the V magnitude in the settling exposure and V_{settled} is the V magnitude in the subsequent settled exposures, so that negative values correspond to the reference stars appearing fainter in the settling image.

Our study also provides a useful statistical context for studies of gamma-ray bursts which show peaks in their optical lightcurves (e.g. Molinari, 2007; Panaitescu & Vestrand,

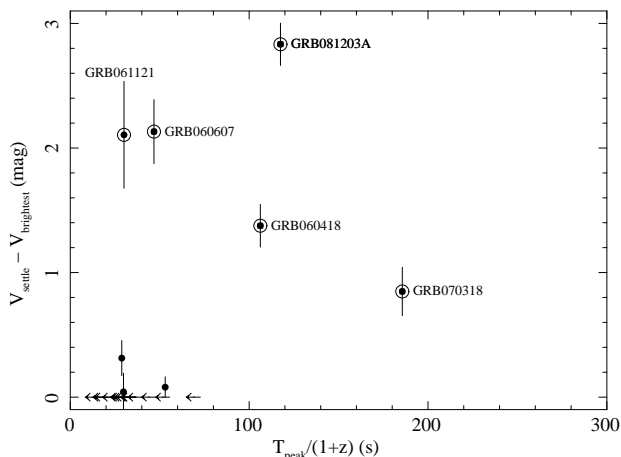


Figure 3. Difference between the brightest magnitude and the settling magnitude for each GRB against the time at which the optical emission peaks, in the rest frame of the GRB. In the majority of cases, the settling exposure records the brightest magnitude (i.e. $V_{\text{settle}} = V_{\text{brightest}}$), hence we have only an upper limit on the time at which the optical emission peaks. GRBs which brighten by more than 0.5 magnitudes after the settling exposure are indicated with large circles and are labelled individually.

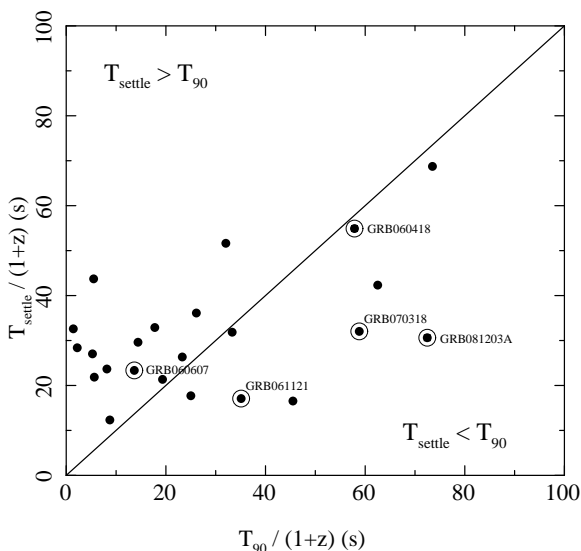


Figure 4. Time T_{settle} at which the settling exposure was taken against T_{90} of the gamma-ray emission. Both times have been converted to the rest frame of the GRB. The solid line indicates equality between T_{settle} and T_{90} . GRBs below the solid line were first observed with UVOT during the T_{90} gamma-ray emitting period, while those above the line were only observed with UVOT after the end of T_{90} . GRBs for which a significant rise in the optical emission is observed are indicated with large circles and labelled individually as in Fig. 3.

2011; Panaitescu, Vestrand & Woźniac, 2013). At the peak-magnitude limit ($V = 16.0$) of our study, only 5 out of 23 GRBs show well-defined optical peaks, or 20 ± 10 per cent, within the time-frame of the observations. The need for even faster optical response times for GRBs is brought into sharp focus: while a significant anti-correlation has been observed between the timing and brightness of the optical peak by Panaitescu & Vestrand (2011) when such a peak is observed, for the majority of GRBs we have only upper and lower limits for these two quantities respectively, because our observations begin too late to measure the optical peak.

Broadly speaking, there are two possibilities for the origin of the optical emission which we observe when the GRB first comes into view of *Swift* UVOT. The optical emission could be produced by the shocks which are generated as the ejecta are slowed by the external medium, and/or the optical emission could be related to prompt gamma-ray emission, which in turn is thought to be produced internally to the outflow. It is possible that a combination of both possibilities could contribute to the observed emission and that the dominant contributor could be different at the time of the settling exposure in different GRBs.

We start by examining the possibility that the earliest optical emission comes from the internal emission. Of our sample of 23 GRBs, there are 14 GRBs for which the settling data were taken after the conclusion of T_{90} ; for these GRBs we can assume that the earliest optical emission is observed too late to be attributed to internal emission. The remaining 9 GRBs, for which T_{90} encompasses the settling exposure, are now examined in more detail. Fig. 5 shows the UVOT and BAT lightcurves for these 9 GRBs. For GRBs 060418, 070318, 081203A, and 090401B, the settling exposure matches well the extrapolation of data from later times, and appears to have little correspondence to the prompt gamma-ray emission. In GRB 090618 the settling exposure shows enhanced optical emission compared to the later time optical lightcurve, and corresponds approximately to one of the peaks in the prompt emission. Therefore the prompt emission could plausibly contribute to the optical flux at the time of the settling exposure for this GRB. In GRB 061007 the settling exposure is consistent with the extrapolation of the UVOT lightcurve, but the UVOT measurement is beyond the bright coincidence-loss limit, and hence we have only a lower limit to the optical flux; the settling exposure coincides with one of the peaks in the prompt emission, so for GRB 061007 we also consider it possible that the prompt emission contributes to the optical flux measured in the settling exposure. In GRBs 061121, 080810 and 081008 the settling exposures correspond to times of little or no gamma-ray emission, but are followed by significant pulses of gamma rays and peaks in the optical that suggest that the optical emission at the time of the settling exposure and for some period subsequently might be related to the prompt emission. Thus there are five GRBs, 061007, 061121, 080810, 081008 and 090618, for which the prompt emission might be contributing to the optical flux at the time of the settling exposure, and/or at the time of the peak optical flux.

We consider next the scenario in which the earliest optical emission comes from the external shock, which is the standard paradigm for the afterglow emission. Either the forward shock propagating into the external medium, or the reverse shock propagating back into the ejecta (Mészáros &

Rees, 1993) are viable mechanisms for producing the early optical emission. Emission from an external shock at an observed time T_{settle} after the beginning of the GRB implies that the external shock is producing detectable optical emission at a distance R_{settle} from the explosion site (Zhang & Meszaros, 2004):

$$R_{\text{settle}} = 2\Gamma^2 c T_{\text{settle}} (1+z)^{-1} \quad (1)$$

where c is the speed of light, z is the redshift of the GRB and Γ is the Lorentz factor of the relativistic outflow. For a characteristic $\Gamma = 300$ and the observed range of $10 \text{ s} < T_{\text{settle}}/(1+z) < 70 \text{ s}$, R_{settle} ranges from 5.4×10^{16} and $3.8 \times 10^{17} \text{ cm}$. For the majority of the GRBs in our sample the optical lightcurve is already declining at the time of the settling observation, so R_{settle} represents an upper limit to the deceleration radius.

In Fig. 4 it is notable that four of the five GRBs for which a robust optical peak is detected have $T_{\text{settle}} < T_{90}$, whereas the majority of the GRBs which are declining in the optical from the first observation have $T_{\text{settle}} > T_{90}$. To evaluate the significance of the apparent trend for a larger proportion of GRBs with optical peaks to have a $T_{\text{settle}} < T_{90}$ than those without, we apply Fisher's exact test, obtaining a p -value of 5.6 per cent for the null hypothesis that there is no trend. The trend is therefore of marginal (approximately 2σ) significance. However, it is interesting to note that two of the GRBs in our sample have observations from ground based observatories which caught the peak of the optical emission: GRB 061007 with ROTSE (Rykoﬀ et al., 2009) and GRB 080319B with TORTORA (Racusin et al., 2008). In both cases, the ground-based observations began before the end of T_{90} ; if these observations were substituted for those of UVOT in Fig. 4 the Fisher's exact test would instead yield a p -value of just 1.8 per cent.

Naturally, it would be expected that the earlier the observations begin, the greater the likelihood of observing the peak in the optical emission, irrespective of T_{90} , so it is worth investigating whether this is responsible for the tendency to observe the peak if $T_{\text{settle}} < T_{90}$. A Komogorov Smirnov (KS) test on the distributions of $T_{\text{settle}}/(1+z)$ for GRBs with and without optical peaks results in a p -value of 99.6 per cent for the null hypothesis that the two distributions are the same, hence the two distributions are indistinguishable. In contrast, a KS test on the distributions of $T_{90}/(1+z)$ for the two groups of GRBs gives a p -value of just 4.8 per cent. This suggests that within our sample, optical peaks are observed preferentially in GRBs with long T_{90} , rather than in GRBs with early optical observations.

Theoretically, the timing of the peak in the optical lightcurve with respect to T_{90} depends on whether the afterglow is produced by the collision of a thin or thick shell with the surrounding interstellar medium. Specifically, the thick shell case corresponds to $\Delta R > (E_K/nm_p c^2)^{1/3} \Gamma_0^{-8/3}$ where ΔR is the thickness of the shell, E_K is the kinetic energy of the shell, Γ_0 is the initial Lorentz factor of the shell, n is the density of the surrounding medium, c is the speed of light in vacuum and m_p is the mass of a proton (Sari & Piran, 1999). It is common to assume that the duration of the burst, T_{90} is approximately $\Delta R/c$, with the implication that for thick shells the peak time of the optical emission should be comparable to T_{90} (Sari & Piran, 1999; Kobayashi, 2000). A peak time for the optical emission which is significantly

Table 2. Parameters for GRBs with well-defined peaks in their optical lightcurves. T_{peak} is the mid-time of the brightest optical measurement, and α is the power-law index of the optical rise, as defined by Equation 2.

GRB	T_{peak} (s)	T_{peak}/T_{90}	α
GRB 060418	264.5	1.84	1.92 ± 0.24
GRB 060607	207.3	3.42	2.83 ± 0.35
GRB 061121	69.5	0.85	3.44 ± 0.71
GRB 070318	340.8	3.15	0.44 ± 0.11
GRB 081203A	358.4	1.62	1.94 ± 0.12

delayed with respect to the end of T_{90} is therefore usually taken to imply the thin shell case (Molinari, 2007; Rykoﬀ et al., 2009). The numerical modelling of Kobayashi & Zhang (2007) would suggest that $T_{\text{peak}}/T_{90} < 2$ may be a realistic expectation for a thick shell. Thick shells should also exhibit relatively shallow afterglow rise profiles, with $\alpha < 1$ where $L \propto t^\alpha$ (Kobayashi, 2000; Kobayashi & Zhang, 2007). For the afterglows with well defined peaks, α can be estimated from the timing and magnitude of the peak relative to the settling exposure:

$$\alpha = \frac{M_{\text{settle}} - M_{\text{peak}}}{2.5(\log_{10} T_{\text{peak}} - \log_{10} T_{\text{settle}})} \quad (2)$$

For the five gamma-ray bursts in our sample for which a secure peak has been observed in the UVOT lightcurve, the values of T_{peak}/T_{90} and α for the rise phase are given in Table 2. None of the GRBs satisfy both $T_{\text{peak}}/T_{90} < 2$ and $\alpha < 1$, implying that all of them have thin shell afterglows. Consequently, if there is a connection between T_{90} and the observability of the optical peak, it is not because the outflows are thick shells.

In the thin shell regime, the peak of the optical emission is expected to occur when the shell reaches the deceleration radius, at which the shell has swept up a mass of material from the surrounding interstellar medium equal to $\sim 1/\Gamma$ times the initial rest mass of the shell (Zhang & Meszaros, 2004). In this case, the timing of the afterglow peak relative to the start of the GRB should be independent of T_{90} , and therefore a connection between T_{90} and the observability of the optical peak emission is not expected in the thin shell case.

An alternative explanation for the trend for GRBs with large T_{90} to present well-defined peaks in their optical emission would be for the prompt emission to be contributing to the optical peak. As we have already discussed, the prompt emission is unlikely to contribute to the observed optical emission except, perhaps, in a small minority of the GRBs in our sample. Of those with well-defined optical peaks, only GRB 061121 (see also Page et al., 2007) is a good candidate for a prompt contribution to the optical peak. Nonetheless, the trend relating T_{90} to detection of optical peaks is based on such a small number of sources, that it could be explained as a combination of prompt optical emission in GRB 061121 together with a statistical fluctuation in these properties amongst the remaining GRBs.

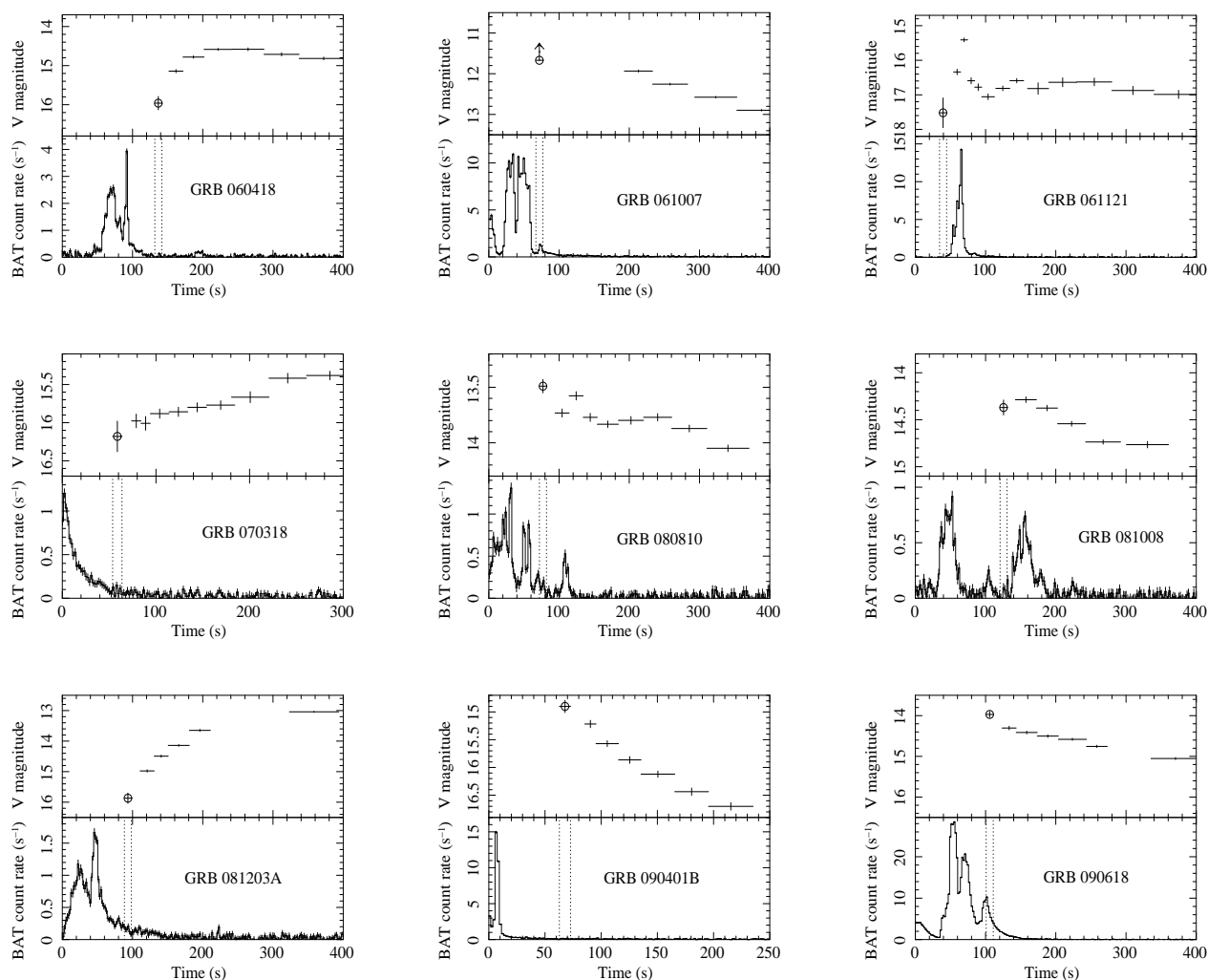


Figure 5. Optical and gamma-ray lightcurves of the 9 GRBs for which T₉₀ extends past the beginning of the UVOT settling exposure. For each GRB the top panel shows the optical lightcurve derived from UVOT and translated into the V band as described in Oates et al. (2012). The settling exposure is indicated with a circle. The bottom panel shows the full-band 15–350 keV lightcurve from the BAT. The dotted lines indicate the time range of the UVOT settling exposure.

5 CONCLUSIONS

We have examined the optical emission from a sample of optically-bright (peak $V < 16$ mag) GRB afterglows as they first came into view with *Swift* UVOT. In one case (GRB 061007) the first second of the settling exposure was excluded because the spacecraft attitude reconstruction was not good enough to prevent trailing of stars at the beginning of the exposure. In another case (GRB 091020) the first second of the settling exposure was excluded because we found evidence that the UVOT photocathode voltage is still ramping up during that first second. The photometric quality of the UVOT settling exposures was verified using photometry of bright stars in the field of view. These stars were found to be of very similar brightness in the settling exposures to subsequent UVOT images (differing on average by 0.021 ± 0.009 mag). The settling exposures are therefore considered to be good enough to derive photometry for the GRB afterglows.

Of the sample of 23 GRBs, all are detected in the UVOT settling exposures, and hence in every case the optical emission had already begun by the time of the settling exposure.

In 9 of the GRBs, the settling exposure took place within T_{90} of the prompt gamma-ray emission. Five GRBs have well defined optical peaks, with measured rises of > 0.5 mag in their optical lightcurves following the settling exposure. A trend is found, with marginal statistical significance (2σ), for these GRBs with well-defined optical peaks to have large values of T_{90} , and to be observed before the conclusion of T_{90} . Such a trend would be expected from thick-shell afterglows, but the timing of their optical peaks and the temporal indices of their optical rises rule out thick-shell behaviour. Instead, a contribution from the prompt emission to the optical peak in one or more GRBs could account for the trend.

ACKNOWLEDGMENTS

This work has been supported by the UK Space Agency under grant ST/P002323/1 and the UK Science and Technology Facilities Council under grant ST/N00811/1. This work has made use of the UK *Swift* Science Data Centre, hosted at the University of Leicester, UK. SRO gratefully

acknowledges the support of a Leverhulme Trust Early Career Fellowship.

References

- Barthelmy S.D., et al., 2005, *Space Science Reviews*, 120, 143
- Breeveld A.A., et al., 2010, *MNRAS*, 406, 1687
- Burrows D.N., et al., 2005, *Space Science Reviews*, 120, 165
- De Pasquale M., et al., 2006, *A&A*, 455, 813
- Fordham, J.L.A., Bone D.A., Read P.D., Norton T.J., Charles P.A., Carter D., Cannon R.D., Pickles A.J., 1989, *MNRAS*, 237, 513
- Gehrels N., et al., 2004, *ApJ*, 611, 1005
- Kobayashi S., 2000, *ApJ*, 545, 807
- Kobayashi S. & Zhang B., 2007, *ApJ*, 655, 973
- Kouveliotou C., 1994, *ApJS*, 92, 637
- Kuin N.P.M. & Rosen S.R., 2008, *MNRAS*, 383, 383
- Mészáros P., Rees M.J., 1993, *ApJ*, 405, 278
- Molinari E., et al., 2007, *A&A*, 469, L13
- Monet D., et al., USNO-A2.0, Flagstaff: US Naval Observatory.
- Oates S.R., et al., 2009, *MNRAS*, 395, 490
- Oates S.R., Page M.J., De Pasquale M., Schady P., Breeveld A.A., Holland S.T., Kuin N.P.M., Marshall F.E., 2012, *MNRAS*, 426, L86
- Page K.L., et al., 2007 *ApJ*, 663, 1125
- Page M.J., et al., 2013, *MNRAS*, 436, 1684
- Panaitescu A., Vestrand W.T., 2011, *MNRAS*, 414, 3537
- Panaitescu A., Vestrand W.T., Woźniac P., 2013, *MNRAS*, 433, 759
- Poole T.S., et al., 2008, *MNRAS*, 383, 627
- Racusin J.L., et al., 2008, *Nature*, 455, 183
- Rees M.J. & Mészáros P., 1992, *MNRAS*, 258, 41
- Rees M.J. & Mészáros P., 1994, *ApJ*, 430, L93
- Rees M.J. & Mészáros P., 2005, *ApJ*, 628, 847
- Roming P.W.A., et al., 2005, *Space Science Reviews*, 120, 95
- Roming P.W.A., et al., 2017, *ApJS*, 228, 13
- Rykoff E.S., et al., 2009, *ApJ*, 702, 489
- Sari R. & Piran T., 1999, *ApJ*, 520, 641
- Zhang B. & Mészáros P., 2004, *International Journal of Modern Physics A*, 19, 2385
- Zhang B., & Yan H., 2011, *ApJ*, 726, 90

APPENDIX A: PHOTOMETRIC PERFORMANCE OF THE UVOT DURING THE SETTLING EXPOSURES

Settling exposures are taken at the final stage of the *Swift* spacecraft slew, when the target has entered the field of view of UVOT, but the spacecraft is still moving. Bright stars observed simultaneously with the GRB afterglows were used to verify the photometric validity of the UVOT photometry used in this study. Source measurements were made using UVOTSOURCE with a five arcsec radius aperture and background measurements were made using the same larger apertures that were employed in the afterglow photometry (Section 2.2). Two measurements were made for each star. The first is from the image formed from the settling data that was used for afterglow photometry. The second measurement was made using the sum of the other *V*-band im-

ages obtained during the same observation sequence of the GRB afterglow, excluding any images exhibiting attitude problems. Photometry obtained from the second measurement is invariably of higher precision than that obtained from the settling data because the exposure times are much longer, and as the photocathode voltage is stable after the settling exposure the photometry is reliable. Table A1 gives the photometry for the stars in each GRB field of view.

We can further examine the photometric performance of the UVOT during the settling exposures by dividing the settling exposure into smaller time bins. In this way, we can investigate whether the photocathode voltage ramp-up is complete, and the detector is stable when the settling exposure begins, or whether the detector performance is changing during the settling exposure. Due to the small integration times involved, this is only practical for the brighter comparison stars. Therefore, for each of the comparison stars in Table A1 brighter than $V = 13$ mag (except for those in the field of GRB 061007)³, we have generated lightcurves with a cadence of 1 s. The lightcurves are shown in Fig. A1.

³ As noted in Section 2.2, there is a problem with the spacecraft attitude reconstruction in the first second of the GRB 061007 settling exposure, and so this is not an appropriate dataset for investigation of the photometric performance at the beginning of the settling exposure.

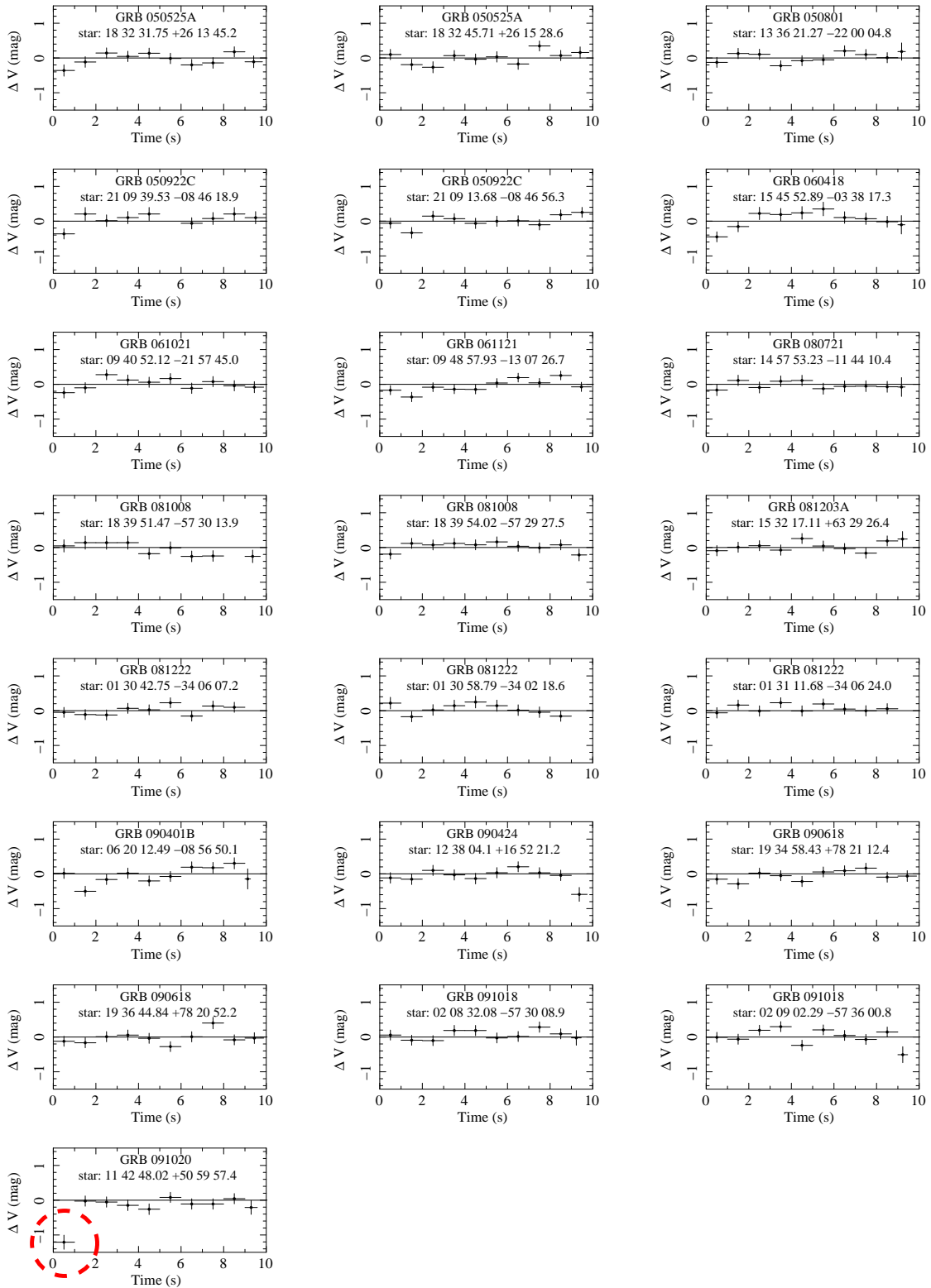


Figure A1 Lightcurves of comparison stars brighter than $V = 13$ mag during the settling exposures. ΔV is computed as $V_{\text{settled}} - V$ where V_{settled} is the V magnitude in the subsequent settled exposures, so that negative values correspond to the reference star appearing fainter in the settling exposure. Note the large, negative ΔV during the first time bin for the GRB 091020 comparison star 11 42 48.02 +50 59 57.4 (indicated by the dashed circle in the bottom left panel), suggesting that the voltage ramp-up of the photocathode took place during the first second of the settling exposure in this case. On two occasions, once each for the two brightest comparison stars (GRB 050922C, star 21 09 39.53 -08 46 18.9 and GRB 081008, star 18 39 51.47 -57 30 13.9) positive fluctuations push the count rate above the bright calibration limit for coincidence loss (Poole et al., 2008; Page et al., 2013). These two datapoints have been omitted from the relevant lightcurves.

Table A1. Photometry of bright stars within the UVOT fields of view for the GRB afterglows used in the study. ΔV is computed as $V_{\text{settled}} - V_{\text{settling}}$ where V_{settling} is the V magnitude in the settling exposure and V_{settled} is the V magnitude in the subsequent settled exposures, so that negative values correspond to the reference star appearing fainter in the settling image.

GRB	Star		V mag in settling data	V mag in subsequent images	ΔV (mag)
	RA (J2000)	dec (J2000)			
GRB 050525A	18 32 31.75	+26 13 45.2	12.95 ± 0.05	12.89 ± 0.02	-0.06 ± 0.06
"	18 32 45.71	+26 15 28.6	12.90 ± 0.05	12.91 ± 0.02	$+0.01 \pm 0.06$
GRB 050801	13 36 21.27	-22 00 04.8	12.26 ± 0.05	12.27 ± 0.02	$+0.01 \pm 0.06$
"	13 36 23.93	-21 59 04.2	14.81 ± 0.10	14.82 ± 0.02	$+0.01 \pm 0.10$
"	13 36 40.88	-21 55 58.7	14.99 ± 0.11	14.85 ± 0.02	-0.14 ± 0.11
GRB 050922C	21 09 39.53	-08 46 18.9	11.71 ± 0.06	11.77 ± 0.02	$+0.06 \pm 0.06$
"	21 09 13.68	-08 46 56.3	12.74 ± 0.05	12.75 ± 0.02	$+0.01 \pm 0.05$
"	21 09 36.04	-08 42 47.8	14.04 ± 0.07	14.00 ± 0.02	-0.04 ± 0.07
GRB 060418	15 45 52.89	-03 38 17.3	11.85 ± 0.06	11.85 ± 0.02	$+0.00 \pm 0.06$
"	15 45 56.35	-03 36 26.3	14.23 ± 0.08	14.17 ± 0.03	-0.05 ± 0.08
"	15 45 48.90	-03 40 17.8	14.19 ± 0.08	14.20 ± 0.03	$+0.01 \pm 0.08$
GRB 060607	21 58 45.54	-22 30 47.9	13.78 ± 0.07	13.83 ± 0.02	$+0.04 \pm 0.07$
"	21 58 53.31	-22 26 31.4	14.14 ± 0.08	14.24 ± 0.02	$+0.11 \pm 0.08$
GRB 060908	02 07 10.34	+00 23 16.6	13.26 ± 0.06	13.15 ± 0.02	-0.11 ± 0.06
"	02 07 20.98	+00 18 44.8	14.44 ± 0.09	14.36 ± 0.02	-0.09 ± 0.09
"	02 07 23.32	+00 20 39.1	15.82 ± 0.16	15.80 ± 0.03	-0.02 ± 0.16
GRB 061007	03 05 01.35	-50 28 19.6	12.60 ± 0.06	12.63 ± 0.02	$+0.03 \pm 0.06$
"	03 05 40.60	-50 31 35.0	13.94 ± 0.08	13.82 ± 0.02	-0.12 ± 0.08
GRB 061021	09 40 52.12	-21 57 45.0	12.68 ± 0.05	12.69 ± 0.02	$+0.01 \pm 0.06$
"	09 40 48.14	-21 55 42.2	13.51 ± 0.06	13.52 ± 0.02	$+0.01 \pm 0.07$
"	09 40 45.48	-22 00 13.9	14.35 ± 0.08	14.14 ± 0.02	-0.21 ± 0.08
GRB 061121	09 48 57.93	-13 07 26.7	12.41 ± 0.05	12.35 ± 0.02	-0.06 ± 0.05
"	09 49 03.24	-13 09 28.4	14.42 ± 0.08	14.40 ± 0.02	-0.02 ± 0.08
"	09 49 04.68	-13 10 31.0	14.63 ± 0.09	14.61 ± 0.02	-0.02 ± 0.09
GRB 070318	03 13 55.40	-42 53 14.1	15.63 ± 0.15	15.53 ± 0.02	-0.10 ± 0.15
"	03 14 10.25	-42 55 32.5	15.53 ± 0.14	15.56 ± 0.02	$+0.03 \pm 0.14$
"	03 13 59.07	-42 57 08.4	15.88 ± 0.17	15.79 ± 0.02	-0.09 ± 0.17
GRB 080721	14 57 53.23	-11 44 10.4	13.00 ± 0.06	12.98 ± 0.02	-0.03 ± 0.06
"	14 58 04.47	-11 41 22.6	15.04 ± 0.11	14.88 ± 0.03	-0.16 ± 0.11
GRB 080810	23 47 05.23	+00 15 45.2	14.02 ± 0.07	14.03 ± 0.03	$+0.00 \pm 0.08$
"	23 46 58.49	+00 18 30.7	14.63 ± 0.09	14.55 ± 0.03	-0.08 ± 0.09
"	23 47 02.82	+00 22 06.9	14.64 ± 0.09	14.71 ± 0.03	$+0.07 \pm 0.09$
GRB 081008	18 39 51.47	-57 30 13.9	11.70 ± 0.06	11.66 ± 0.03	-0.05 ± 0.06
"	18 39 54.02	-57 29 27.5	12.30 ± 0.05	12.33 ± 0.02	$+0.02 \pm 0.06$
"	18 40 00.95	-57 27 17.5	14.22 ± 0.08	14.24 ± 0.03	$+0.03 \pm 0.08$
GRB 081203A	15 32 17.11	+63 29 26.4	12.60 ± 0.05	12.63 ± 0.02	$+0.03 \pm 0.06$
"	15 31 51.63	+63 29 47.6	13.70 ± 0.07	13.61 ± 0.03	-0.10 ± 0.07
"	15 32 27.45	+63 32 34.2	15.26 ± 0.12	14.88 ± 0.03	-0.38 ± 0.13
GRB 081222	01 30 58.79	-34 02 18.6	11.89 ± 0.06	11.92 ± 0.02	$+0.03 \pm 0.06$
"	01 30 42.75	-34 06 07.2	12.47 ± 0.05	12.47 ± 0.02	$+0.00 \pm 0.06$
"	01 31 11.68	-34 06 24.0	12.70 ± 0.05	12.78 ± 0.02	$+0.08 \pm 0.06$
GRB 090401B	06 20 12.49	-08 56 50.1	12.13 ± 0.05	12.08 ± 0.02	-0.05 ± 0.06
"	06 20 21.95	-08 59 30.1	13.66 ± 0.07	13.58 ± 0.02	-0.07 ± 0.07
"	06 20 16.32	-08 59 48.6	13.62 ± 0.07	13.61 ± 0.02	-0.01 ± 0.07

Table A1. continued

GRB	Star RA (J2000)	dec (J2000)	V mag in settling data	V mag in subsequent images	ΔV (mag)
GRB 090424	12 38 04.01	+16 52 21.2	12.84 ± 0.05	12.78 ± 0.03	-0.06 ± 0.06
"	12 38 08.61	+16 50 23.9	14.15 ± 0.08	14.10 ± 0.03	-0.05 ± 0.07
"	12 37 50.82	+16 50 11.7	14.10 ± 0.08	14.18 ± 0.03	$+0.08 \pm 0.08$
GRB 090618	19 36 44.84	+78 20 52.2	12.17 ± 0.05	12.11 ± 0.02	-0.05 ± 0.06
"	19 34 58.43	+78 21 12.4	12.62 ± 0.05	12.56 ± 0.02	-0.06 ± 0.06
"	19 36 34.28	+78 19 20.7	14.27 ± 0.08	14.16 ± 0.02	-0.11 ± 0.08
GRB 090812	23 32 36.14	-10 39 02.2	14.39 ± 0.08	14.28 ± 0.04	-0.11 ± 0.09
"	23 33 01.04	-10 37 06.4	15.35 ± 0.13	15.14 ± 0.05	-0.21 ± 0.14
"	23 32 40.95	-10 36 11.2	16.00 ± 0.18	15.98 ± 0.07	-0.01 ± 0.19
GRB 091018	02 08 32.08	-57 30 08.9	12.22 ± 0.05	12.29 ± 0.02	$+0.06 \pm 0.06$
"	02 09 02.29	-57 36 00.8	12.51 ± 0.05	12.53 ± 0.02	$+0.02 \pm 0.06$
"	02 08 50.91	-57 33 58.0	14.43 ± 0.09	14.46 ± 0.02	$+0.03 \pm 0.09$
GRB 091020	11 42 48.02	+50 59 57.4	12.88 ± 0.05	12.68 ± 0.02	-0.20 ± 0.06
"	11 43 07.16	+50 57 28.8	15.21 ± 0.12	15.17 ± 0.02	-0.04 ± 0.12
"	11 42 47.24	+50 57 24.2	15.49 ± 0.14	15.59 ± 0.02	$+0.10 \pm 0.14$
GRB 100906A	01 54 31.65	+55 40 14.7	13.29 ± 0.06	13.27 ± 0.02	-0.02 ± 0.06
"	01 54 38.13	+55 37 14.5	13.31 ± 0.06	13.31 ± 0.02	$+0.00 \pm 0.06$
"	01 55 00.63	+55 38 55.3	13.66 ± 0.07	13.62 ± 0.02	-0.05 ± 0.07